Experiments and modelling of multiple sequential MeV ion irradiations and deuterium exposures in tungsten

M. Pečovnik[*a], T. Schwarz-Selinger[b], S. Markelj[a]

[a]*Jožef Stefan Institute, Jamova cesta 39, 1000 Ljubljana, Slovenia*

[b]*Max-Planck-Institut für Plasmaphysik, Boltzmannstrasse 2, D-85748 Garching, Germany*

Abstract

Bulk tungsten samples were irradiated sequentially with 20 MeV tungsten ions and exposed to deuterium plasma. The experiments were performed in order to simulate the displacement damage that fusion neutrons will cause in a tungsten plasma-facing component of a future fusion device. To study the influence of the presence of hydrogen isotopes during the creation of displacement damage on the final defect density, tungsten irradiation and deuterium decoration cycles were performed up to three times. Deuterium depth profiling with ^{3}He Nuclear Reaction Analysis and Thermal Desorption Spectroscopy showed that the deuterium concentration increased after each additional tungsten irradiation and deuterium exposure. After the third cycle, the deuterium concentration reached a maximum of 3.6 at.% at the given plasma exposure temperature of 370 K. We attribute this increase in retention to the stabilization of the displacement damage during the tungsten irradiation by the presence of deuterium.

The experimental results were simulated using the MHIMS-R macroscopic rate-equation code, which was recently upgraded with a damage stabilization term to describe experiments where tungsten was irradiated with MeV tungsten ions and simultaneously exposed to low-energy deuterium ions. Using this novel model, it was possible to quantitatively describe also the present results for the sequential irradiation/exposure scheme, with model parameters that were congruent with parameters derived from the simultaneous experiment. Modelling shows that kinetic de-trapping of trapped deuterium takes place during irradiation However, it is not the dominant process that explains defect stabilization. In addition, the model facilitates the extrapolation of present experimental results to an even larger number of sequential tungsten irradiation and deuterium exposure cycles. The model predicts that after about five sequential irradiation and plasma exposure cycles, a stationary state is reached with an associated maximum trapped D concentration of 4.2 at.% for the given exposure temperature of 370 K.

Keywords: tungsten, deuterium retention, displacement damage, damage model, damage stabilisation

The content of this manuscript is identical to an article with the same title published in Journal of Nuclear Materials Volume 550 (2021) 152947
https://doi.org/10.1016/j.jnucmat.2021.152947

[*]Corresponding author: matic.pecovnik@ijs.si

1. Introduction

In future fusion reactors such as ITER and DEMO, strict limitations on in-vessel tritium retention are imposed as tritium is radioactive and poses a public health and safety concern. As tungsten (W) exhibits low intrinsic hydrogen isotope (HI) retention and other favourable material properties such as high melting temperature, it is currently the material of choice for the divertor section of ITER and will most probably be the basis for the plasma-facing components of DEMO.

However, HI retention in W plasma-facing components will be increased by several orders of magnitude by HI trapping in lattice defects. While some defects, such as grain boundaries, dislocations and others occur in the material naturally, many more will be created by 14 MeV neutron irradiation originating from the D + T fusion reaction [1], [2]. As predicted by rate equation modelling, tritium inventory in these defects will be the main contribution to the entire tritium inventory of the W plasma-facing components [3]. Because of the neutrons high energy and lack of electric charge they will cause displacement damage throughout the entire material depth with projected displacement per atom (dpa) levels of several dpa per year [1], [2]. The neutrons will also cause wall-material transmutation and activation.

Because neutrons with energy as high as 14 MeV are created only in conditions present in a fusion reactor, there is an obvious lack of laboratory experiments that can take the effect of 14 MeV neutron irradiation on HI retention into full account. Usually fission neutron irradiation [4] or heavy ion MeV irradiation are used to create displacement damage [5]–[7]. As fission neutron irradiation also causes material transmutation and activation, this makes the samples difficult to handle. Therefore, it is preferable to use heavy ion MeV irradiation. Such irradiation has been shown to be a good proxy for studying the effect of neutron irradiation on HI retention [8], [9] excluding transmutation and in-wall helium production effects. Experiments that study HI retention in displacement-damaged W are usually conducted in the following way: (1) The samples are irradiated with MeV heavy ions (often W irradiation is used, e.g. [6], [7], [10], [11]) to produce the displacement damage, (2) after the irradiation, the displacement damage is decorated with deuterium (D) with various exposure means such as plasma, atom or ion exposure at various exposure temperatures, (3) this D decoration allows us to investigate the depth distribution of the underlying displacement damage using Nuclear Reaction Analysis (NRA) and to determine the kinetics of D desorption from the various lattice defect types using Thermal Desorption Spectroscopy (TDS). However, such sequential experiments cannot take possible synergies

between D retention and displacement damage creation into account. Recently, it has been shown that the amount of displacement damage created during W ion irradiation is strongly influenced by the presence of HI during damage creation and by the local damaging temperature [12]–[14].

These recent experiments used two different approaches to study this interesting effect. The experiments presented in [12] and [13] used an approach where the displacement damage is created by a simultaneous MeV W ion irradiation and low-energy D ion/atom exposure. Although the experimental results of such experiments are very well suited for extrapolation to reactor conditions, where displacement damage will also occur via simultaneous neutron irradiation and D/T exposure, such experiments require a sophisticated and dedicated experimental setup which is able to measure the fluxes and fluences of both D and W ions and also has the ability of controlling the temperature of the sample while maintaining high vacuum. However, it is limited to elevated exposure temperatures (above ~500 K) as it is based on the diffusion of HIs into the depth during the exposure. Another approach, which was used in [14] uses multiple sequential W irradiations and D exposures. Such an approach is more easily executable in many laboratories that have experience with MeV heavy ion irradiation and D ion/plasma/atom/molecule exposure. This procedure allows to extend the investigations to lower temperatures as it is based on the HIs trapped in the lattice before creating the additional displacement damage and hence the HI diffusion depth and the damage depth are decoupled from each other. However, the experimental results derived from a sequential approach cannot be extrapolated to reactor conditions as easily as the ones derived from the simultaneous approach. It should be noted that the extrapolation can still be done by analysing the results using macroscopic rate equation (MRE) models. Such extrapolations have recently become even more attainable with the development of a MRE model of displacement damage creation and stabilization [15]. Such a model was developed and successfully applied to determine the stabilization effect of D in the simultaneous experiment described in [12]. Still, its applicability for other experimental conditions remained untested.

In this work we will present a continuation of the sequential experiment presented in Ref. [14]. There, an experiment with up to two consecutive sequential W ion irradiations and D plasma exposures was carried out. The experimental results showed that because of D presence during the second W ion irradiation, the amount of D retained in the sample after the second sequential W irradiation and D exposure increased by almost a factor of two, compared with the amount of trapped D found before the second irradiation. Modelling of the increase in D retention

after the second consecutive sequential W irradiation and D exposure was already presented in [14]. However the modelling did not try to explain the reason for the increased retention. Instead, the experimental results were described by ad-hoc adding more lattice defects that were created by the second W irradiation. To see if the trend of increasing D retention would continue with even more consecutive sequential W irradiations and D exposures, we proceed here by sequentially W irradiating and D exposing for three consecutive times. To elucidate the experimental findings of the results reported in [14] and the complementary experimental results of the present study, we use our MRE approach that is able to model the creation of displacement damage by W ions and the so-called stabilization induced by the presence of D during the irradiation of the material [15]. After determining the model parameters, we apply the approach to extrapolate the experiment to an even larger number of sequential W irradiation and D exposure steps to determine the maximum D concentration expected in such an experiment.

As this work is a direct continuation of the previous work, we will take the liberty of quickly summarizing the findings presented in [14] before moving on to the new results.

2. Experiment

In the combined experimental set, which will be referred to from now on as *sequential multi-damaging*, 99.97 wt.% purity polycrystalline W samples were sequentially W irradiated and exposed to a well-defined D plasma. 20 MeV W irradiation was performed to a fluence of $\Phi = 7.87 \times 10^{17}$ W/m^2 which produced a primary damage dose of 0.23 dpa according to SRIM [16] (Quick Calculation of Damage option, 90 eV displacement damage energy, evaluating the "vacancy.txt" output). The W irradiation was always carried out at room temperature (295 K). Such an irradiation dose is expected to be sufficient to achieve the saturation of D concentration in almost the entire damage depth when W irradiation occurs in hydrogen-free W [5], [17]. To minimize defect concentrations and hence minimize deuterium uptake beyond the self-damaged zone, samples were annealed at 2000 K for two minutes prior to the first W irradiation. After each W irradiation, the self-damaged samples were exposed to a well-controlled D plasma with < 5 eV/D energy and an ion flux of $\Gamma = 5.6 \times 10^{19}$ D/m^{2}s. During the exposure, which served to populate the previously created defects with D, the samples were kept at a constant temperature of 370 K. A series of exposures with increasing D fluence revealed that at this temperature and D ion energy, D decorates the complete range of the self-damaged zone of roughly 2 μm for a D fluence of

1.5×10^{25} D/m^2. Longer D exposure do not lead to further changes in the D depth profile (see also Fig. 1 in [14]). More details of the experiment are described in [14] and references therein.

A schematic representation of the sequential multi-damaging experiment is shown in Fig. 1. The first sample was W irradiated and D loaded only once to serve as a benchmark of displacement damage creation without D presence (single damaging). The second sample was additionally W irradiated after the first D exposure which produced displacement damage beyond expected saturation levels [5] due to D-induced defect stabilization (double damaging) [12]–[15], [18]. The additional displacement damage created was decorated with D by a second D plasma exposure. A third sample was sequentially W irradiated and D plasma loaded for a third consecutive time (triple damaging) to experimentally determine if the D retained in the sample would rise even more by continuing this sequential W irradiation and D exposure scheme. For each W irradiation and D exposure cycle, all parameters were kept the same, meaning D and W fluxes, fluences, energies and temperatures were identical for all cases.

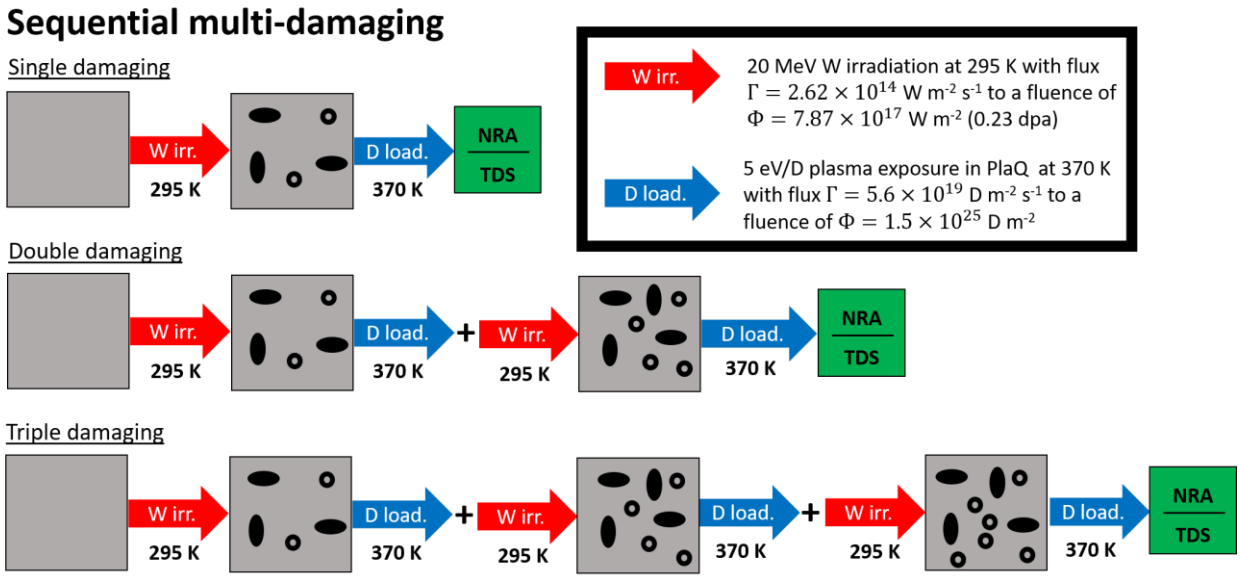

Figure 1: The experimental summary scheme of the sequential multi-damaging experiment. 20 MeV W irradiation was utilized to create displacement damage in the W samples at 295 K after which the created defects were decorated using a D plasma exposure at 370 K.

After each D plasma loading step of the samples, the D depth profile was measured using Nuclear Reaction Analysis (NRA). The time span between plasma exposure and NRA varied between four to nine days. It is important to note that self-damaged samples do not show significant outgassing or so-called 'dynamic retention' unlike plasma- or ion beam exposed undamaged samples [19]. A

recent dedicated study of D retention in self-damaged tungsten (single damaged) showed that some small loss of D of a few percent could only be detected in the first days. For longer times the D amount stayed constant within the accuracy of the NRA method [8]. To make sure this also holds true for multiply-damaged samples an identical double damage sample was prepared and analysed with NRA first six days after D exposure and again 400 days after D exposure. No significant difference neither in the shape of the depth profile nor in the total D concentration beyond the accuracy of the method was found. To determine the desorption kinetics of D, which allows to infer the amount of D trapped in specific defect types, all samples were also analysed using Thermal Desorption Spectroscopy (TDS) with a controlled temperature ramp equal to 3 K/min after the last D plasma exposure and NRA analysis. The details of the measuring and analysis techniques can also be found in [14]. Sample temperature measurement for the present triple damage sample was improved compared to the previous measurements of the single- and double-damaged samples. Initially, the temperature response of the samples to the linear oven temperature ramp was calibrated afterwards in independent experiments by a thermocouple spot-welded to a tungsten sample of identical size and surface finish. For the triple-damaged sample however, a shielded thermocouple was touching the sample surface during the TDS ramp. Afterwards the response of this shielded thermocouple to the linear oven temperature ramp was checked against a thermocouple spot-welded to the tungsten. This reduced the inaccuracy of the temperature measurement to a value below 10 K.

3. Experimental results

The D depth profiles of the single-, double- and triple-damaged sample are presented in Fig. 2a. We would like to stress that the raw data for the single-damaged and double-damaged samples are the same as in Ref. [14]. However, the depth profiles shown here are the result of a more accurate re-evaluation of the raw data with a slightly different energy calibration, as the D depth profile shown in [14] for the double damaged sample suffers from an unphysical feature at 0.5 μm. Several single-damaged as well as one double damaged sample were prepared since 2018 with identical parameters. The shapes of the depth profiles of these samples are identical to the ones shown in Fig. 2. Additionally, the concentrations were identical within the stated reproducibility of 5 %.

For reference, the D profile of a non-W-irradiated tungsten sample that was prepared in the same way and D exposed to the same fluence at the same temperature as the other three samples is

shown in Fig. 2a in addition (magenta line). Besides an areal density of 2×10^{17} D/m^2 close to the surface very little D is retained inside the samples. The bulk D concentration of 2×10^{-3} at.% is close to the detection limit for the selected measurement parameters. One can see, that the D plasma does not create any defects but only decorates the existing ones. Compared to this undamaged sample, the D concentration for all three self-damaged samples is high up to the maximum damage depth defined by the SRIM calculated primary damage distribution shown in grey. Deeper in the samples the D concentration falls to values comparable to the undamaged W sample. Up to the maximum damage depth, the D depth profile is relatively flat for all cases. However, a rise in D concentration can be seen in the 0.2-1.5 μm depth range, which correlates with the depth range that received a larger damage dose due to the shape of the SRIM calculated primary damage distribution. The observed rise with a relative increase in D concentration of 10-15 %, is quite small. This suggests that displacement damage dose of 0.11 dpa, that is achieved near the surface and near the maximum damage depth range, is indeed close to saturation as predicted by Refs. [5], [17]. The relative flatness of the D depth profile in the entire damage zone also means that the D fluences used in the experiment were large enough to populate all of the defects created by the W irradiation for all three W irradiations. This means that we can assume that the D depth profile is directly proportional to the underlying defect depth profile. The observed features are not determined by the depth resolution [20].

From Fig. 2a we can also see that the D concentration consistently grows with further W ion irradiations and D decoration cycles. It increases from 1.6 at.% to 2.8 at.% when the sample is W irradiated and D loaded twice and grows further to 3.6 at. % after the third irradiation cycle. In terms of relative D concentration increase, the D concentration increases by a factor of 1.7 after the second sequential W irradiation and D exposure and 1.3 after the third sequential W irradiation and D exposure. By extrapolating this trend to further sequential W irradiations and D exposures we can infer that the D concentration would eventually saturate. However, this saturation seems to be quite slow, as with a combined W irradiation fluence equal to 2.36×10^{18} W/m^2 (0.69 dpa) the D concentration still rose after the third sequential W irradiation and D exposure. This value is much larger compared to the 0.1-0.2 dpa that is observed for W irradiation of hydrogen-free tungsten [5], [17].

The D desorption spectra for the single-, double- and triple-damaged samples are shown in Fig. 2b. The desorption behaviour of D is consistent throughout all of the three analysed samples.

The D desorption starts at around 400 K, which is in line with the D exposure temperature of 370 K. All D is desorbed at a temperature of around 950 K, which is consistent with other experiments [10], [21]–[23]. In some of the listed literature data, the temperature at which all D was desorbed was a bit higher, reaching 1000 K [6], [24]. This is due to the fact that a faster heating rate was used in those cases.

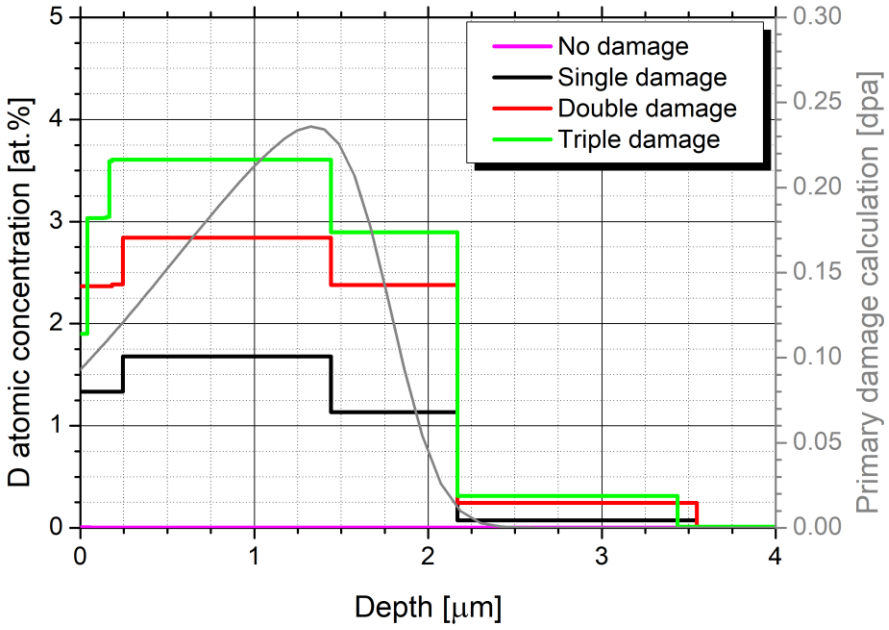

(a)

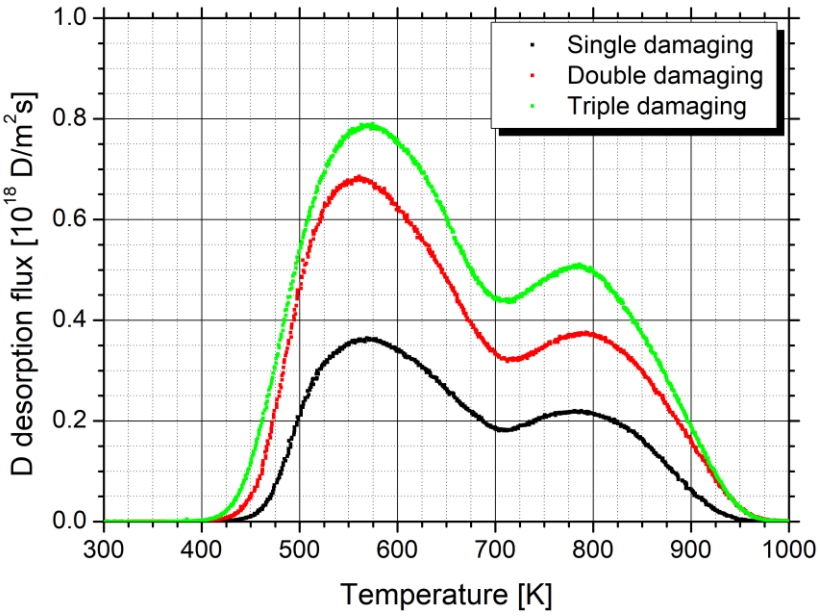

(b)

Figure 2: The experimental results of the sequential multi-damaging experiment are shown. D depth profiles for all three damaging cycles are shown in (a). Additionally, the sample which was not W-irradiated and was only exposed to D plasma at 370 K is also shown. Alongside the D depth profiles, the SRIM calculated primary damage distribution is shown in grey. The D depth profile of the single- and double-damaged sample is a more accurate re-evaluation of the raw data shown in Ref. [14]. *The D desorption spectra are shown in (b).*

The majority of D is desorbed in two broad peaks centered at 550 K and 780 K in all three cases. The most prominent change in the D desorption if more W irradiations and D decoration cycles are used is the increase of the overall amount of D that is desorbed during the TDS and the relative intensity of both desorption peaks. However, the change in the relative intensity of the D desorption peaks with additional W/D cycles is also important. This relative intensity is defined as the ratio of intensity of the high temperature desorption peak divided by the intensity of the low temperature peak. From the data these are calculated to be 0.60, 0.55, 0.65 for the single-, double- and triple-damaging, respectively. This changing of the relative intensities suggests that there are multiple defect types present in the samples that are responsible for D retention and that each has an independent probability to be stabilized by the trapped D.

4. Simulation

To simulate the results of the experiment we used the macroscopic rate-equation code MHIMS-R [3] which is based upon the fill-level dependent HI-defect interaction picture. In this description, each defect type can trap several HI at the same time. The number of trapped HI defines the so-called fill-level of the defect. Each fill-level has an associated de-trapping energy. In contrast, in the classical HI-defect interaction picture each defect can only trap a single HI and the de-trapping energy of D depends solely on the defect type.

The code has recently been updated by including a displacement damage creation [18] and D stabilization model [15]. As mentioned before, for hydrogen-free tungsten it has been shown experimentally, that defect densities increase initially with damage level but saturate above approximately 0.1-0.2 dpa [5], [17]. This is considered by modelling displacement damage creation as an exponential function with a saturation concentration – $n_{i,max}$ – for each defect type *i* [15], [18]. The presence of D allows the defect concentrations to reach beyond this value through D-induced stabilization. The creation-stabilization model [15] can be summarized by the following equation:

$$\frac{dn_i(x,t)}{dt} = \frac{\Gamma\eta\ \theta(x)}{\rho}\left[1 - \frac{\mathrm{n_i}(x,t)}{\mathrm{n_{i,max}}}\left(1\ -\ \alpha_i \frac{\mathrm{n_i}(x,t) -\ n_i^0(x,t)}{\mathrm{n_i}(x,t)}\right)\right] \quad (1)$$

Here $n_i(x,t)$ is the depth- and time-dependent concentration of defect type i. Γ is the flux of impinging W particles, $\theta(x)$ the SRIM-calculated primary damage profile and ρ the density of tungsten. η = 1.5 × 10^9 m^{-1} is the probability of an impinging W particle to create a defect per unit length [15]. We assume it is the same for all defect types. Our choice of η = 1.5 × 10^9 m^{-1} means that the defect concentrations saturate between 0.1-0.2 dpa as determined experimentally by various experiments where no D is present during the displacement damage creation process [5], [17]. The stabilizing effect of D on the defects is modelled through the α_i parameter. α_i defines the new defect saturation value and is the so-called stabilization parameter. Besides α_i, the rate of defect creation depends on the number of defects filled with hydrogen. This is expressed by the difference between n_i and n_i^0, the latter being the concentration of empty defects.

Equation 1 can be interpreted as follows: D that is trapped in defects leads to a higher amount of defects that survive the W irradiation process. An explanation for this would be that defects that are occupied by D have a lower probability to annihilate. For vacancies, this interpretation is motivated by density functional theory calculations that showed that D trapped in a vacancy inhibits (to a certain extent) annihilation of this vacancy with the neighbouring crowdion-type self-interstitial atoms in W [25]. For vacancy clusters, the mechanism in W has not yet been made clear by atomistic simulations. However, in bcc Fe, trapped HI was shown to inhibit vacancy cluster dissociation [26] by increasing the binding energies of vacancies to the vacancy cluster. With fewer vacancy clusters dissociating, the overall concentration of vacancy clusters is higher in a HI-containing sample, which we interpret as HI-induced stabilization. A similar effect could be possible in W which also has a bcc crystal lattice although this has not yet been confirmed. Unfortunately, these two are the only ab initio atomic simulations that investigate D-induced stabilization of lattice defects to the knowledge of the authors.

Stabilization by trapped D is somewhat in contradiction with the understanding how displacement damage occurs in W. During irradiation by W ions, displacement damage predominantly occurs in dense cascades. The local temperature of these cascades is much higher than the temperature required to de-trap a D. Therefore, the D trapped very near the cascade are most likely thermally de-trapped. Such a microscopic picture suggests that our macroscopic model

that is based on trapped D inducing stabilization does not seem to be in line with the microscopic reality. However, this is not necessarily the entire picture. As was reported in [14], no D is lost during the consecutive W irradiation but stays in the sample. Therefore, D must be very effectively re-trapped. Hence, one of the possible reconciliations between the microscopic and macroscopic views is as follows: During a cascade many vacancy-SIA pairs are created. The vacancies are not very mobile [27] and most likely stay near the place of their creation. However, their corresponding SIAs are much more mobile and can quickly diffuse through the W lattice, even far away from the place where they were created. Sooner or later, they will encounter another vacancy that was created by a previous cascade or a different location of the present cascade. Due to the high mobility of the SIA, the encountered vacancy can be far away enough from the current cascade that it is not affected by the local extreme temperature. This means that it is still very likely for the older vacancy to hold some trapped D and can therefore still be stabilized.

Another addition to the MHIMS-R code is the inclusion of so-called kinetic de-trapping. The parametrization of this process is described in more detail in Ref. [15]. Its importance for our modelling efforts will be highlighted in the discussion section.

We must also describe our choice of solute D boundary conditions. As the energy of impinging D ions in the plasma exposure of sequential multi-damaging is enough for them to penetrate directly into the W bulk we use the Dirichlet boundary conditions $c_m(x = 0) = 0$. This means that the D implantation flux is modelled as a volume source of solute D in the bulk. The distribution of the source is calculated with SRIM and is modelled as a Gaussian distribution with a projected mean range of 0.7 nm and a lateral dispersion of 0.5 nm for the 5 eV/D plasma exposure.

When fitting the experimental data, we focused on fitting the D desorption spectra. The simulated D depth profile is only considered as an output and was not used for fitting, as the maximum damage depth is already defined by the W irradiation itself and is fully considered by our choice of $\theta(x)$. Also, the D concentration is implicitly considered in the amount of overall D desorption, as the overall D retention as determined by TDS and NRA are in good agreement. This was shown to be the case in Ref. [14]. To determine the quality of each fit of the experimental D desorption spectrum we will use the reduced chi square as a figure of merit. It is defined as:

$$\chi^2_{red} = \frac{1}{N-1}\sum_{i=1}^{N}\frac{\left(\Gamma_i^{sim} - \Gamma_i^{exp}\right)^2}{\sigma_i^2} \quad (2)$$

N is the number of points in the experimental desorption spectra. Γ_i^{exp} is the experimental desorption flux at a temperature T_i and similarly Γ_i^{sim} is the simulated desorption flux at T_i. σ_i is the experimental error of D desorption at temperature T_i. It was determined directly from the D desorption measurement count rates, assuming that the relative error follows Poisson statistics $\sigma_I(\text{count}) = (\Gamma_i^{exp}(\text{count}))^{-1/2}$. Another error that we must consider comes from the relative error for the particle fluxes derived from the drift and fluctuations of the quadrupole signal while dosing a constant amount of D_2 into the chamber with a calibrated leak bottle. This error was experimentally determined to be about 1-2 %. The χ^2_{red} calculation was limited to TDS temperatures between 450 and 900 K. In this desorption temperature range, 90 % of retained D was desorbed for all samples.

5. Simulation results

Before continuing with the comparison between the simulation and experiment we would like to stress the procedure by which we attempted to fit the experimental results. In the first step, the saturation concentrations – $n_{i,max}$ – and de-trapping energies of all defects produced by the W irradiation were determined by fitting the D desorption spectrum of the single-damaged sample. As a second step, the stabilization parameter for each defect type – α_i – is determined by fitting the double damaging D desorption spectrum. These are determined without changing the de-trapping energies and saturation concentrations that were determined from the single-damaged D desorption spectrum. This defines all of the free parameters of the simulation. These were then used to predict the D desorption spectrum of the triple damaging sample. They were also used to determine the simulated D depth profiles which can be compared to the experimental ones for all three W/D cycles.

Three distinct defect types were used with several fill-levels each when the model was applied for the simultaneous experiments in Ref. [15]. We have decided to also use three defect types for the present sequential procedures here, but because the D exposure in the current experiment was done at a lower temperature than in [12], [15] we had to use more fill levels to

adequately fit the D desorption at lower temperatures. A summary of the parameters used to fit the single-damaged sample is:

- Defect type 1 with concentration $n_{1,max}$ = (0.22±0.01) at.% and fill-level energies (1.08±0.03, 1.16±0.02, 1.25±0.02, 1.34±0.02, 1.46±0.03) eV,
- Defect type 2 with concentration $n_{2,max}$ = (0.29±0.02) at.% and fill-level energies (1.68±0.02, 1.86±0.01) eV,
- Defect type 3 with concentration $n_{3,max}$ = (0.05±0.01) at.% and fill-level energy (2.05±0.01) eV.

The reported energies are associated with an exponential pre-factor equal to 10^{13} s^{-1}. Such an approach constrains the model parameters so they are not entirely 'free'. A diffusion energy barrier of 0.2 eV [28] and a pre-factor equal to 1.9×10^{-7} m^2 s^{-1} [28] were used in the simulation as determined for H. As D is used in our experiment, the pre-factor for H was scaled by $\sqrt{2}$ to account for the difference in masses. The given de-trapping energy error bars reflect the variation of de-trapping energies to obtain the best fit for the three different experiments. The temperature uncertainty associated with the de-trapping energy uncertainty is between 10-20 K for the 3 K/min ramp used in our experiments. The uncertainty in defect concentration determination comes mainly from the uncertainties in determining the experimental D retention. To elaborate on the choice of our fitting parameters we show a fit of the simulation to the D desorption spectrum of the single-damaged W sample in Fig. 3.

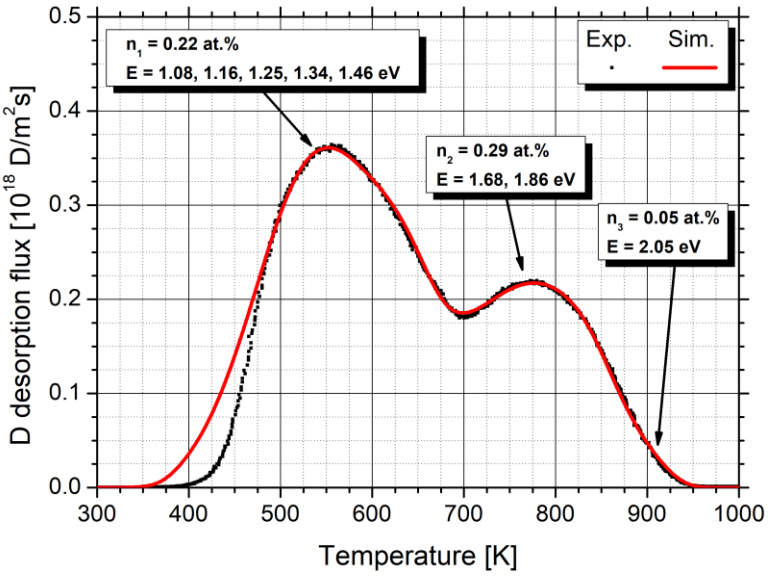

Figure 3: Simulated (red line) and experimental (black dots) D desorption spectra of the single-damaged sample, which highlights the choice of the fitting parameters that are independent of D-induced stabilization. Three defect types are used each with several fill-levels.

It is clearly seen that the simulation fits the single-damage D desorption spectrum very well, but one failure is apparent. The simulation overestimates D desorption in its beginning in the 400-450 K range. The reason for this is unknown. We have tried eliminating the 1.08 eV fill-level of defect type 1, but this still leads to some overestimation in the 400-420 K range and underestimation in the 420-450 K range. As such an overestimation is a common occurrence in the literature [7], [10], [11], [14], [18], [29] we have decided to keep the 1.08 eV fill-level, while keeping in mind that this overestimation will also lead to an overestimation of the D concentrations in the comparison with the experimental D depth profiles. This overestimation is in the 5-10 % range, depending on each specific case. This overestimation is also the reason why the calculation of the reduced chi square is based on the 450-900 K TDS temperature range and not on the entire D desorption measurement range.

The comparison between the simulations and the experimental results for the entire experimental set are shown in Fig. 4. In Fig. 4a the comparison between the simulated and experimental D desorption spectra are shown, while in Fig. 4b the D depth profiles are shown.

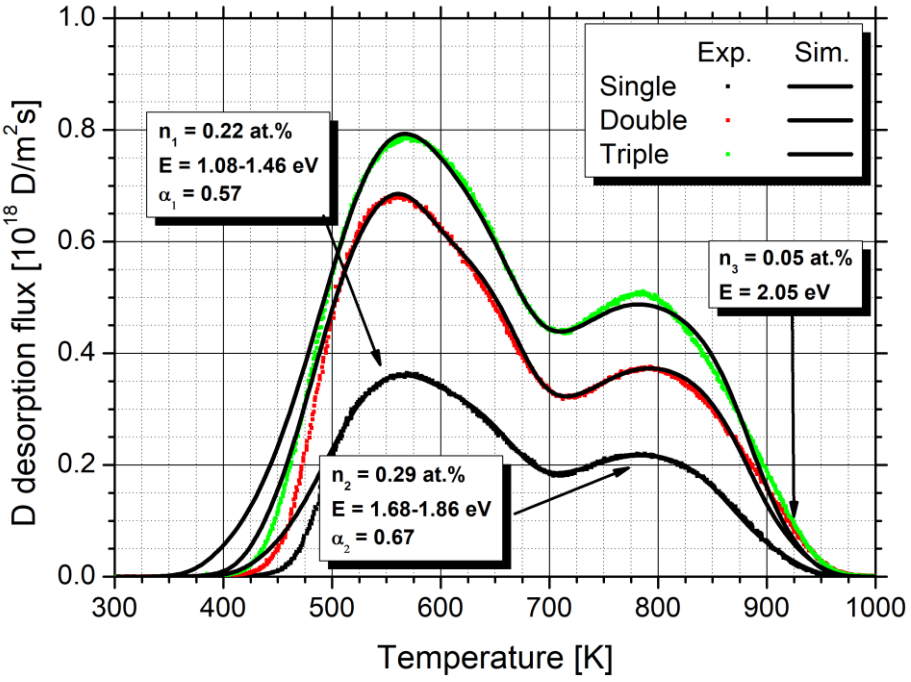

(a)

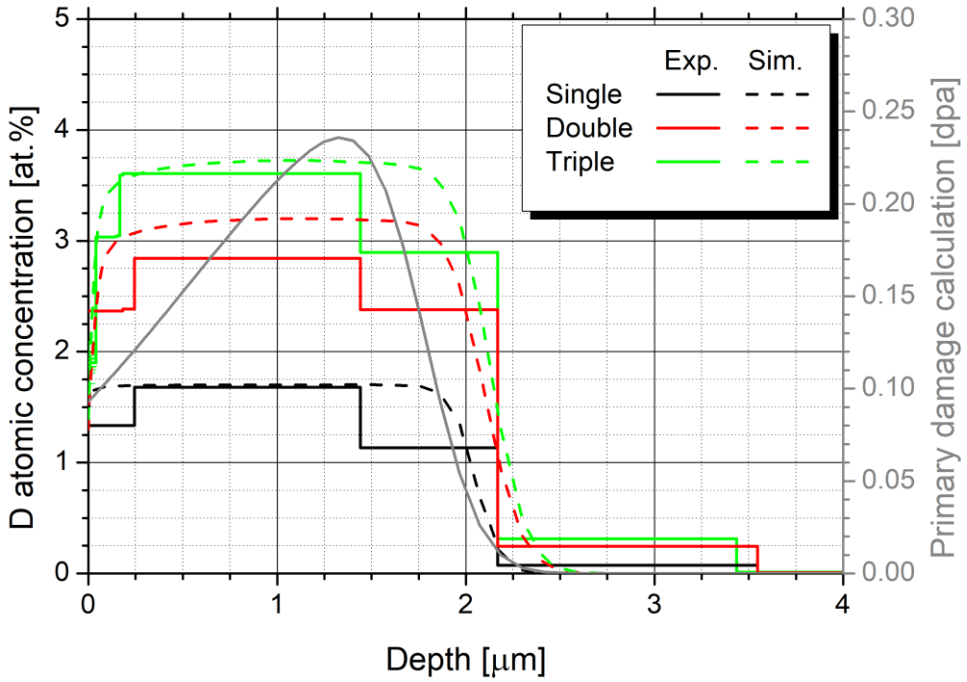

(b)

Figure 4: Comparison of simulation and experiment for the D desorption spectra (a) and D depth profiles (b).

As we have only used the D desorption spectra to obtain the simulation parameters we will start by analysing their fits. We see that beside the obvious overestimation of D desorption in the 400-450 K range already seen in Fig. 3, the simulation fits the experiment for all three cases very well. To achieve such a fit of the double-damage experimental result we have used stabilization parameters for defect type 1 and 2 of $\alpha_1 = 0.57 \pm 0.03$ and $\alpha_2 = 0.67 \pm 0.03$, respectively. No appreciable stabilization of defect type 3 was observed, therefore, we have set $\alpha_3 = 0$. A similar result was also achieved in [15]. Small changes of the α_1 and α_2 parameters for the second and third W irradiation were allowed within the experimental error of the desorption measurement. This uncertainty was determined to be in the 5% range, which results in the given error bars for the α_1 and α_2 parameters. We can see that despite the fact that only minimal changes were allowed, the simulation parameters derived from the single and double damaging recreate the experimental results for the triple damaging D desorption spectrum very well. The reduced chi square resulting from fitting the simulation to the experiment are 0.88, 0.92 and 0.98 for the single, double and triple damaging, respectively.

The simulation of the D desorption spectrum also resulted in corresponding D depth profiles. The comparison between the simulation-derived and experimental D depth profiles are

shown in Fig. 4b. As shown, the measured depth profiles match very well, despite the fact that no fitting was performed. The maximum damage depth and D depth profile shape are well reproduced at the same time, despite the fact that the D depth profile is much flatter than the SRIM-calculated primary damage profile. This indicates that the choices of the SRIM-defined $\theta(x)$, the value for the probability of damage creation $\eta = 1.5 \times 10^9$ m^{-1} and the saturation concentrations $n_{i,max}$ were chosen appropriately. The D concentration in the D depth profiles is slightly overestimated in all cases, which is due to the early rise of desorption at low temperature (400-450 K) present in the simulation as described earlier. We can see that the higher D concentration at depths between 0.2–1.5 μm is also replicated by the simulation. As was already pointed out in the experimental results section, this is mostly due to the shape of the SRIM calculated damage dose depth distribution.

In the simulation we can see a decrease in D concentration near the surface for the triple-damaged sample. This decrease in D concentration is attributed to the interplay between kinetic de-trapping and D-induced stabilization. As W ions create displacement damage, they also de-trap normally tightly bound D trapped in defects [14], [15]. If this happens in the depth of the material, the D will be promptly re-trapped in nearby defects. However, if this happens near the surface, the likelihood of the D desorbing from the sample becomes quite large. This means that defects in close proximity to the surface are mostly empty of D during the W irradiation. This of course means that D cannot induce stabilization. Therefore, no additional defects are created. The fact that this is observed in the experimental results of the triple damaging and is successfully reproduced in the simulation brings further validity to the consistency of our experimental results and the validity of the displacement damage creation and stabilization model. To determine if the surface feature in the triple-damaged sample is only a result of NRADC overfitting, the data from an annular detector has also been analysed which has been shown to have a five-time better depth resolution [20]. The feature was still produced by the NRADC fit, which makes us confident that the feature is real. As seen from the simulation of the double-damaged sample the same near-surface feature is expected. However, this feature cannot be observed in the experimental D depth profile. Data from an annular detector for the single- and double-damaged samples is unfortunately not available. However, the D depth profiles of the single- and double-damaged samples have been carefully re-evaluated with a more precise energy calibration. As the feature could still not be resolved, it is unclear at this time if the feature could not be measured because of a lack of counting statistics/depth resolution or if it is simply not there.

6. Discussion

Before going into the discussion about the implications of the simulation results we would like to also mention the seemingly large number of model parameters that were used for the simulation. In total there were fourteen parameters.

Firstly, in our previous work on displacement damage creation during simultaneous D exposure [15] as well as defect annealing [22] very similar sets of model parameters have been derived. Those simulation efforts showed that a relatively large number of model parameters was needed to adequately describe the experimental results, as only such a large number of model parameters allowed us to describe the variations in D desorption spectra for e.g. various sample temperatures. In Ref. [15] we have discussed how the derived fill-level energies compare to various atomistic simulations and experimental findings found in the literature. In Ref. [21] a similar discussion was presented, this time focusing on the evolution of defects at elevated temperatures. To summarize those findings, defect type 1 has been tentatively attributed to single-vacancies, defect type 2 to small vacancy clusters and defect type 3 to large vacancy clusters. The parameters are hence not entirely 'free' as they can be connected to some physical meaning.

Secondly, it is important to note that the minimum number of model parameters is three parameters (defect concentration, at least one fill-level de-trapping energy and a stabilization parameter) per defect type. This means, that the fundamental choice which determines the number of model parameters is the number of defect types and the number of fill-levels for each defect type. In principle a similar quality fit of the single-damaged D desorption spectrum could also be achieved by using a smaller number of defect types and number of fill-levels. For instance, in Ref. [14] the results were described by a single defect with five fill-levels with de-trapping energies of (1.18, 1.32, 1.46, 1.70, 1.84) eV and a defect concentration for each W/D cycle. The high-temperature D desorption shoulder, herein attributed to defect type 3, was ignored in Ref. [14]. As two different defect concentrations were used to describe the experimental behaviour no stabilization parameter was needed. In total there were seven model parameters. However, when trying to describe the results of double damaging, they could not reproduce the results with the same fit quality. Most importantly, there was no predictive capability in their modelling in contrast to the present model: For the triple damaging an additional defect density would have been need, hence a new and in this case actually 'free' parameter would have been necessary. In the present work, the triple damaging was correctly reproduced with the parameters derived from the results

of the single- and double-damaged sample without the addition of a free parameter. In addition, they could not reproduce the fact that the D desorption in the low-temperature desorption peak increased more than the D desorption in the high-temperature peak after the second W/D cycle. This can only be explained by the fact that several defect types are present in the material. This is the most important justification for the number of model parameters used in our simulation.

Lastly, we have tried to limit over-fitting of our simulation by limiting the parameters that can be changed when describing the results of each W/D cycle. For instance, the de-trapping energies of the fill-levels and defect densities (in total eleven parameters) were completely defined by the fit of the single-damaged sample. The stabilization parameters (the remaining three parameters) were defined by the fit of the double-damaged sample. This means that the ability of the parameters to generalize outside of the scope where they were defined was tested twice for the defect densities and de-trapping energies and once for the remaining stabilization parameters. As we have seen, we were able to reproduce our results to a very good degree despite these restrictions, which provides further justification for our use of the number of model parameters. Furthermore, we were able to predict the D depth profiles for all samples from the parameters determined by fitting the D desorption spectra.

6. 1. Kinetic de-trapping

Let us first touch upon the impact of kinetic de-trapping on our simulation results. In the initial simulation in [14] the effect of stabilization was attributed to be a consequence of kinetic de-trapping which causes some D to be de-trapped and to enter the solute D population during W irradiation. The solute D was thought of as being responsible for stabilization of defects. In the present simulation, the same results could be simulated by the fact that D is trapped in defects during the second or third damaging. Therefore, in principle kinetic de-trapping is not needed to reproduce the stabilization behaviour. For this reason, we will discuss here what is the role of kinetic de-trapping in our simulation.

From the reduction of D concentration near the surface observed in the simulation and also in the triple damaging experiment, kinetic de-trapping is expected to have an important role in de-populating D from defects. As discussed before, this effect should be most important in the very near-surface region, as the kinetically de-trapped D is likely to desorb from the sample. However, in the bulk of the sample, the impact of kinetic de-trapping is expected to be less important for the

amount of trapped D, as kinetically de-trapped D is likely to be promptly re-trapped in either pre-existing or new defects. To quantify the interplay between kinetic de-trapping and re-trapping we have extracted information from the simulation about the occupation ratios of different fill-levels of defect type 1 immediately before and after the second W irradiation. These are shown in Fig. 5a and 5b, respectively.

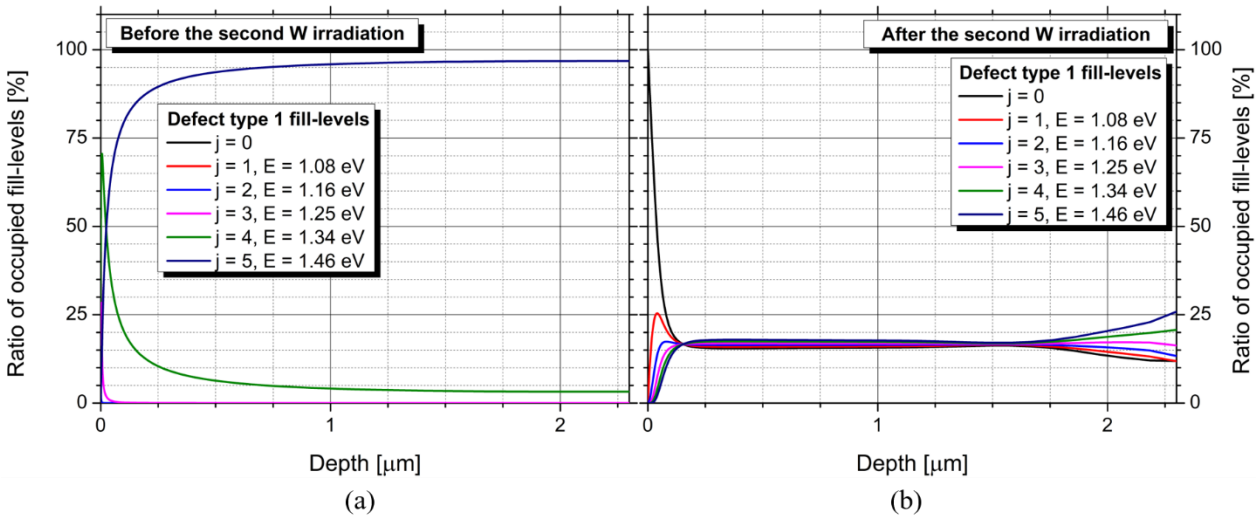

Figure 5: Occupancy ratios of defect type 1 immediately before (a) and after (b) the second W irradiation.

As one can see, immediately before the second W irradiation (Fig. 5a), the majority of defect type 1 has five trapped D (*j = 5)* with only a minority of four trapped D (*j = 4)*. The other fill-levels are not occupied. Also, it is important to note that no empty defect type exists (*j = 0*). It is interesting to see that the fill-level behaviour of defect type 1 changes, when we are close to the surface even before W irradiation. This is because, some D is redistributed among fill-levels very near the surface after the D plasma is shut-off and the sample is cooling from 370 K to 300 K. Immediately after the second W irradiation (Fig. 5b) the fill-level occupancy ratios are very different compared to the ones before the second irradiation. We can see that near the surface almost 100 % of defects of type 1 are empty of D as we have discussed in the previous sections. This means that right next to the surface, no stabilization of defects could occur. Further into the bulk, it seems that all fill-levels are equally filled. On average, 16% of defects of type 1 are empty (*j = 0*). Of course, one expects a similar behaviour in the other two defect types. According to the simulation, at the end of the second W irradiation, 32% and 50% of defect type 2 and 3, respectively, hold no D (not shown).

To get a sense of what this means for the values of stabilization parameters used in the simulation, we performed simulations with and without kinetic de-trapping. The notable differences between both simulations were:

- Simulation without kinetic de-trapping could not reproduce the reduction of D concentration near the surface observed in the triple damaging experiment,
- In the simulation without kinetic de-trapping, the α parameters had to be reduced by 10 % on average to achieve the same maximum D concentration in the bulk compared to when kinetic de-trapping is included. Note that this percentage is not the same as the percentage of empty defects at the end of the second W irradiation. This is because a majority of stabilization occurs at the beginning of the second W irradiation, when many defects are still filled, due to the exponential saturation behaviour of displacement damage creation.

Based on the observations above, we can state that while kinetic de-trapping is important to properly describe stabilization both in terms of shape and concentration, it is not the driver of stabilization. According to equation 1, the trapped D amount is the driver of stabilization.

6. 2. Saturation of displacement damage

So, what is then the main player in this rather different experimental scenario as compared to the simultaneous W/D irradiation [15] and does one expect a saturation of defect creation when D is present? From the experimental results one can suspect that saturation of the displacement damage has not yet occurred even after three consecutive W irradiation and D exposure procedures. Here, saturation is understood in the context that if another cycle of W irradiation and D exposure was performed, no further increase of D concentration would be measured. As we have seen in the simulation section the model behaved very well in replicating the experimental results. Therefore, it has been used to extrapolate the experimental results to even more consecutive sequential W irradiation and D exposure cycles to determine the final saturation of displacement damage for our specific experimental conditions. One should keep in mind that other experimental conditions, especially other W irradiation or D exposure temperatures, could lead to different D concentration saturation values.

As a reminder, the extrapolation uses the saturation concentrations of individual defects in hydrogen free tungsten – $n_{i,max}$ – which were determined from the single-damaged sample and the stabilization parameters – α_i – of the defects that were determined from the double damage sample

and confirmed by the triple damage sample. We have then continued with the W irradiation and D exposure cycles by adding additional cycles on top of the third one. The goal of the extrapolation is to define a *final saturation concentration* – $n_{i,sat}$ – which would occur after a sufficient number of consecutive sequential W irradiations and D exposures. One should also note that the simulation at zero cycles starts at almost zero D concentration. This is the case as the maximum D concentration in the bulk of a sample that was only exposed to PlaQ at 370 K was approximately $2x10^{-3}$ at.% as shown in fig. 2.

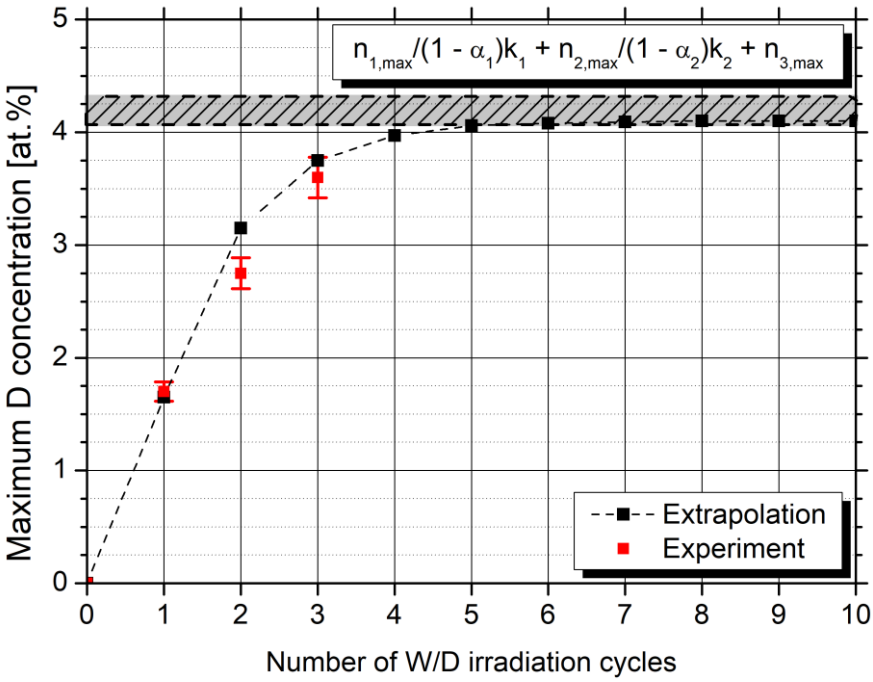

Figure 6: Experimental and simulated maximum D concentration as a function of consecutive sequential W irradiations and D exposures using the displacement damage creation and stabilization model. Extrapolation shows that final D saturation occurs at approximately five consecutive sequential W irradiation/D decoration cycles. The confidence interval for the maximum concentration was derived with equation 14 varying the simulations parameters within their uncertainties and is plotted as a striped band.

The evolution in maximum D concentration with each additional sequential W irradiation and D exposure based on the MHIMS-R simulation with the parameters derived before in section 5 is shown in Fig. 6. One can see that D concentration saturation occurs after approximately five sequential W irradiation and D exposure cycles for a combined W fluence of 3.94×10^{18} W/m^2 (1.15 dpa). The corresponding saturation D concentration is determined to be 4.2±0.1 at.%, the uncertainty originating from the uncertainty of the α and n_{max} parameters.

Now let's try to understand how stabilization of displacement damage occurs at every W irradiation/D exposure step. After the first W irradiation step the defect concentration is equal to $n_{i,max}$. Further W irradiation would not change the defect density as we reached the saturation value for hydrogen-free tungsten already where defect creation and annihilation balance each other. Afterwards, all of these defects are decorated with D. During the second W irradiation, again $n_{i,max}$ defects are created. A portion of them annihilates while another portion is stabilized due to trapped D. This means some additional damage survives after the second W irradiation, which would not occur if D was not trapped in the defects.

Let's calculate the steady-state concentration of defect type *i* during the second W irradiation as this determines the amount of additional damage created. We denote steady-state concentration as $n_i^{(2)}$. Steady state is achieved when equation 1 is equal to 0. This means:

$$1 - \frac{n_i^{(2)}}{n_{i,max}} \left(1 - \alpha_i \frac{n_i^{(2)} - n_{i,0}}{n_i^{(2)}} \right) = 0 \tag{3}$$

At the beginning of the W irradiation the concentration of non-empty defects was equal to $n_{i,max}$. Although we have shown that kinetic de-trapping has a meaningful effect on D redistribution among defects and fill-levels, a majority of stabilization occurs at the beginning of the W irradiations due to the exponential saturation nature of defect creation. Because of this and in order to make the calculation easier, we assume that the concentration of non-empty defects is constant throughout the W irradiation and is equal to all available defects after the first W irradiation, in other words $n_i^{(2)} - n_{i,0} = n_{i,max}$. This means we can write equation 3 as:

$$1 - \frac{n_i^{(2)}}{n_{i,max}} \left(1 - \alpha_i \frac{n_{i,max}}{n_i^{(2)}} \right) = 0 \tag{4}$$

From simulations with and without kinetic de-trapping, we know that using this assumption we make an error of about 10%. Solving equation 4 for $n_i^{(2)}$ we get:

$$n_i^{(2)} = n_{i,max}(1 + \alpha_i) \tag{5}$$

This means that during the second W irradiation an additional $\Delta n_i{}^{(2)} = \alpha_i n_{i,max}$ of defects survive. Afterwards, all of the defects created so far are decorated after the second D exposure. This means that at the beginning and throughout the third W irradiation the concentration of non-empty defects is equal to $n_i^{(2)}$. We can continue in this manner by calculating steady state concentration after the third cycle $n_i^{(3)}$:

$$1 - \frac{n_i^{(3)}}{n_{i,max}}\left(1 - \alpha_i \frac{n_i^{(2)}}{n_i^{(3)}}\right) = 0. \tag{6}$$

By solving equation 6 for $n_i^{(3)}$, we get:

$$n_i^{(3)} = n_{i,max} + \alpha_i n_i^{(2)} = n_{i,max}(1 + \alpha_i + \alpha_i^2). \tag{7}$$

Now we begin to see a pattern. For the *l*-th D decoration/W irradiation cycle, the amount of created lattice defects will behave as a geometric series:

$$n_i^{(l)} = n_{i,max} \sum_{j=0}^{l-1} \alpha_i^j \tag{8}$$

We can see that after the first W irradiation, defect concentration increases by $n_{i,max}$. After the second W irradiation the concentration increases by $\alpha_i n_{i,max}$ and by an additional $\alpha_i^2 n_{i,max}$ after the third irradiation. This means that we can also write an equation that defines a steady state concentration of defect type *i* after *l* W irradiation as:

$$n_i^{(l)} = n_i^{(l-1)} + \alpha_i^{l-1} n_{i,max} \tag{9}$$

This means that the effect of stabilization by trapped D becomes smaller and smaller as we increase the number of W/D cycles. As the stabilization parameters α_i are smaller than 1, the geometric series in equation (8) converges to a finite value. When the number of W/D cycles goes to infinity the sum defines the final saturation value, which is equal to:

$$n_{i,sat} = \frac{n_{i,max}}{1 - \alpha_i} \tag{10}$$

We will highlight the usefulness of this calculation by using it on the experimental D depth profile data. By doing this we can estimate the α_i parameters directly from the measured D concentrations. As stated in the experimental results section, the D concentration was equal to 1.6 at. % after one cycle, 2.8 at. % after two cycles and 3.6 at. % after three cycles. This means that based on equation 8 we can write:

$$c_2 = c_1(1 + \alpha) \rightarrow \alpha_{2-1} = 0.75 \tag{11}$$

$$c_3 = c_2 + c_1\alpha^2 \rightarrow \alpha_{3-2} = 0.71 \tag{12}$$

While these are slightly larger than the ones derived from the MHIMS-R simulation, this is somewhat expected as we have used the D concentrations from the experiment instead of the derived defect concentrations. This was done as the defect concentrations are of course not directly available from the experimental data. Also, keep in mind the 10 % estimated error we make when using this analytical approach, where we essentially neglect the effect of kinetic de-trapping. Still, the derived stabilization parameters are fairly close to the simulation-derived ones.

Using equation 10, we can calculate the D concentration in the material, once final saturation occurs. As all of the defects fill-levels are almost completely filled due to the low D exposure temperature (see Fig. 5a), the concentration captured in each defect can be calculated as:

$$c_i = n_{i,sat}k_i, \tag{13}$$

where k_i is the number of available fill-levels for defect type *i*. The entire concentration *c* of D trapped in the self-damaged zone of the sample is a sum of the trapped D concentration in each defect:

$$c = \frac{n_{1,max}k_1}{(1 - \alpha_1)} + \frac{n_{2,max}k_2}{(1 - \alpha_2)} + n_{3,max}. \tag{14}$$

Our previous findings that there are three defect types present in the sample which are responsible for the majority of D retention is already considered in equation 14. We have also included our findings that defect type 3 only has one fill-level and that $\alpha_3 = 0$. The D concentration calculated with equation 14 at final saturation is included in Fig. 6 as a striped band. The upper and lower limit of the band are based on the uncertainties derived for the densities and the stabilization parameters.

The calculated final D saturation concentration of 4.2 at.% is close to the values found in our previous experiments, when simultaneous W irradiation/D ion exposure was performed at slightly higher temperature [12], [15]. There we have found that when simultaneous W irradiation/D exposure occurs at 450 K and the D re-exposure after W irradiation is done at 450 K, a saturation D concentration of approximately 2.2 at.% is expected based on an extrapolation similar to the one used in this work. Additionally, in Ref. [15] we speculated that a saturation D concentration of 3 at.% would be measured if simultaneous W irradiation/D exposure would occur at room temperature and the created defects were populated with a D ion re-exposure at 450 K. While this prediction is less than the saturation determined here, one should consider that in this experiment D exposure occurred at 370 K. This lower temperature of exposure means that more fill-levels of defect type 1 are filled during the D exposure if the exposure is performed at 370 K (five fill-levels are filled) as compared with 450 K (two fill-levels are filled), thus increasing the measured D concentration. Taking all of this into account, we can see that our stabilization model has considerable predictive capability even when generalizing the results of an experiment with a specific set of experimental parameters (D ion energy, D exposure type, exposure temperature, irradiation temperature, W ion energy) to experiments with seemingly vastly different experimental designs.

Additionally, we would like to stress that while the predicted high D concentrations are worrying they need further elaboration when it comes to their applicability in a future fusion device such as DEMO. Firstly, let's address the fact that in our study 20 MeV W ions were used to create displacement damage, while in DEMO 14 MeV neutrons will be the root cause of displacement damage creation. The neutrons will cause W wall transmutation which could affect various aspects of hydrogen isotope retention. Unfortunately, this cannot be studied with MeV W irradiation. Therefore, we cannot make any statements on how transmutations would affect the stabilization

behaviour of the material. Meanwhile, the displacement damage creation aspect of neutron irradiation has been shown to be well reproduced by MeV W irradiation [8], [9]. Therefore, we speculate that the HI stabilization behaviour observed in this and other studies [12]–[15], [18] can be reliably extrapolated from experimental W ion irradiations to fusion neutron irradiation. Secondly, one should note the high D concentration observed in the experiment was the result of W irradiation at room temperature and 370 K D exposure. Of course, in ITER and DEMO, the wall will be heated to much higher temperatures by the plasma-wall interaction. However, near the cooling elements, the wall temperature is expected to be much lower, enabling HI to be retained in the defects. Furthermore, in the plasma-exposed areas of future reactors such as the divertor, the solute HI concentrations will be much higher due to the HI fluxes which will be orders of magnitude higher compared to the ones used in this work [30] thus promoting stabilization. Dedicated experiments at higher fluxes will have to be performed at elevated temperatures to test the applicability of the present model also in this parameter range.

5. Conclusion

In a previous experiment, W samples were sequentially irradiated with W ions and exposed to D plasma for one and two consecutive times in order to determine the effect of D on displacement damage [14]. The experiment found that the D concentration rises from 1.6 at.% to 2.8 at.% when the W sample is sequentially irradiated for a second time compared to a single sequential irradiation. During a slow heating ramp of 3 K/min the D has been found to desorb predominantly in two distinct and independent desorption peaks centered at 550 K and 780 K. Although the experiment produced valuable information on the magnitude of the D-induced stabilization for the experimental conditions used, it had no predictive capability.

In this work we have presented a continuation of the previous experiment. A W sample was treated in the same manner as the W samples in the original experiment, with the addition of another, third sequential W irradiation and D exposure cycle. This was done to see if a saturation of concentration of D was reached after the second irradiation sequence or if D concentration would increase even further when a third W irradiation and D exposure cycle was performed. A further increase in D concentration from 2.8 at.% to 3.6 at.% has been measured after the third consecutive sequential irradiation. The shape of the D desorption spectrum remained similar after the third

irradiation with only the overall D desorbed was increased in accordance with the rise of D concentration found in the D depth profile.

The complete experimental dataset of single, double and triple sequential W irradiation and D exposure cycles was simulated by using a macroscopic rate equation model of displacement damage creation and stabilization [15]. The experimental D depth profiles and desorption spectra were successfully described with a single set of model parameters. Afterwards we have used those parameters to extrapolate to even more consecutive sequential W irradiation and D decoration cycles in order to determine a saturation D concentration value. We have determined that after approximately five consecutive sequential W irradiation and D decoration cycles a D saturation concentration of 4.2 at. % is expected. Additionally, the successful use of the displacement damage creation and stabilization model, originally developed to describe the simultaneous W irradiation and D ion exposure scheme [12], on a different experimental scheme proves the applicability and validity of the model. This observation bolsters the confidence in the general observation that defect concentrations and consequently HI retention is substantially larger when displacement damage is created while HI are present.

Acknowledgement

This work has been carried out within the framework of the EUROfusion Consortium and has received funding from the Euratom research and training programme 2014-2018 and 2019-2020 under grant agreement No 633053. The views and opinions expressed herein do not necessarily reflect those of the European Commission. The authors acknowledge the support from the Slovenian Research Agency (research core funding No. P2-0405). We thank Wolfgang Jacob for his interest in this work and the diligent reading of the manuscript.

References

[1] J. H. You, “A review on two previous divertor target concepts for DEMO: Mutual impact between structural design requirements and materials performance,” *Nucl. Fusion*, vol. 55, no. 11, p. 113026, 2015.

[2] Y. Hatano *et al.*, “Deuterium trapping at defects created with neutron and ion irradiations in tungsten,” *Nucl. Fusion*, vol. 53, no. 7, p. 073006, 2013.

[3] E. A. Hodille *et al.*, “Study of hydrogen isotopes behavior in tungsten by a multi trapping

macroscopic rate equation model," in *Physica Scripta*, 2016, vol. 2016, no. T167, p. 014011.

[4] M. Shimada *et al.*, "The deuterium depth profile in neutron-irradiated tungsten exposed to plasma," *Phys. Scr. T*, vol. T145, pp. 1–6, 2011.

[5] O. V. Ogorodnikova and V. Gann, "Simulation of neutron-induced damage in tungsten by irradiation with energetic self-ions," *J. Nucl. Mater.*, vol. 460, pp. 60–71, May 2015.

[6] M. J. Simmonds *et al.*, "Reduced deuterium retention in simultaneously damaged and annealed tungsten," *J. Nucl. Mater.*, vol. 494, pp. 67–71, Oct. 2017.

[7] A. Založnik, S. Markelj, T. Schwarz-Selinger, and K. Schmid, "Deuterium atom loading of self-damaged tungsten at different sample temperatures," *J. Nucl. Mater.*, vol. 496, pp. 1–8, 2017.

[8] B. Wielunska, M. Mayer, T. Schwarz-Selinger, A. E. Sand, and W. Jacob, "Deuterium retention in tungsten irradiated by different ions," *Nucl. Fusion*, vol. 60, p. 096002, 2020.

[9] W. R. Wampler and R. P. Doerner, "The influence of displacement damage on deuterium retention in tungsten exposed to plasma," *Nucl. Fusion*, vol. 49, no. 11, p. 115023, 2009.

[10] M. Pečovnik, S. Markelj, A. Založnik, and T. Schwarz-Selinger, "Influence of grain size on deuterium transport and retention in self-damaged tungsten," *J. Nucl. Mater.*, vol. 513, pp. 198–208, 2019.

[11] M. J. Simmonds, T. Schwarz-Selinger, J. H. Yu, M. J. Baldwin, R. P. Doerner, and G. R. Tynan, "Isolating the detrapping of deuterium in heavy ion damaged tungsten via partial thermal desorption," *J. Nucl. Mater.*, vol. 522, pp. 158–167, 2019.

[12] S. Markelj *et al.*, "Displacement damage stabilization by hydrogen presence under simultaneous W ion damage and D ion exposure," *Nucl. Fusion*, vol. 59, no. 8, p. 086050, Aug. 2019.

[13] S. Markelj *et al.*, "Deuterium retention in tungsten simultaneously damaged by high energy W ions and loaded by D atoms," *Nucl. Mater. Energy*, vol. 12, pp. 169–174, Aug. 2017.

[14] T. Schwarz-Selinger, J. Bauer, S. Elgeti, and S. Markelj, "Influence of the presence of deuterium on displacement damage in tungsten," *Nucl. Mater. Energy*, vol. 17, pp. 228–234, Dec. 2018.

[15] M. Pečovnik, E. A. Hodille, T. Schwarz-Selinger, C. Grisolia, and S. Markelj, "New rate equation model to describe the stabilization of displacement damage by hydrogen atoms during ion irradiation in tungsten," *Nucl. Fusion*, vol. 60, no. 3, 2020.

[16] J. Ziegler, "SRIM." [Online]. Available: http://srim.org/.

[17] V. K. Alimov *et al.*, "Deuterium retention in tungsten damaged with W ions to various damage levels," *J. Nucl. Mater.*, vol. 441, no. 1–3, pp. 280–285, Oct. 2013.

[18] E. A. Hodille *et al.*, "Stabilization of defects by the presence of hydrogen in tungsten: simultaneous W-ion damaging and D-atom exposure," *Nucl. Fusion*, vol. 59, no. 1, p. 016011, Jan. 2018.

[19] R. Bisson *et al.*, "Dynamic fuel retention in tokamak wall materials: An in situ laboratory study of deuterium release from polycrystalline tungsten at room temperature," *J. Nucl. Mater.*, vol. 467, pp. 432–438, Dec. 2015.

[20] B. Wielunska, M. Mayer, and T. Schwarz-Selinger, "Optimization of the depth resolution for deuterium depth profiling up to large depths," *Nucl. Instruments Methods Phys. Res. Sect. B Beam Interact. with Mater. Atoms*, vol. 387, pp. 103–114, Nov. 2016.

[21] O. V. Ogorodnikova, B. Tyburska, V. K. Alimov, and K. Ertl, "The influence of radiation damage on the plasma-induced deuterium retention in self-implanted tungsten," in *Journal of Nuclear Materials*, 2011, vol. 415, no. 1 SUPPL, pp. S661–S666.

[22] M. Pečovnik, S. Markelj, M. Kelemen, and T. Schwarz-Selinger, "Effect of D on the evolution of radiation damage in W during high temperature annealing," *Nucl. Fusion*, vol. 60, p. 106028, 2020.

[23] S. Markelj, T. Schwarz-Selinger, M. Pečovnik, W. Chrominski, A. Šestan, and J. Zavašnik, "Deuterium transport and retention in the bulk of tungsten containing helium: The effect of helium concentration and microstructure," *Nucl. Fusion*, vol. 60, no. 10, 2020.

[24] A. Založnik *et al.*, "The influence of the annealing temperature on deuterium retention in self-damaged tungsten," in *Physica Scripta*, 2016, vol. 2016, no. T167, p. 014031.

[25] D. Kato, H. Iwakiri, Y. Watanabe, K. Morishita, and T. Muroga, "Super-saturated hydrogen effects on radiation damages in tungsten under the high-flux divertor plasma irradiation," *Nucl. Fusion*, vol. 55, no. 8, p. 083019, Aug. 2015.

[26] E. Hayward and C. Deo, "Energetics of small hydrogen-vacancy clusters in bcc iron," *J. Phys. Condens. Matter*, vol. 23, no. 42, p. 425402, Oct. 2011.

[27] S. K.-D., Rasch; R. W., Siegel; H., "Quenching and recovery investigations of vacancies in tungsten," *Philos. Mag. A*, vol. 41, no. 1, pp. 91–117, 1980.

[28] N. Fernandez, Y. Ferro, and D. Kato, "Hydrogen diffusion and vacancies formation in

tungsten: Density Functional Theory calculations and statistical models," *Acta Mater.*, vol. 94, pp. 307–318, Aug. 2015.

[29] E. A. Hodille *et al.*, "Simulations of atomic deuterium exposure in self-damaged tungsten," *Nucl. Fusion*, vol. 57, no. 5, p. 056002, May 2017.

[30] E. A. Hodille *et al.*, "Retention and release of hydrogen isotopes in tungsten plasma-facing components: The role of grain boundaries and the native oxide layer from a joint experiment-simulation integrated approach," *Nucl. Fusion*, vol. 57, no. 7, p. 076019, Jul. 2017.

CRediT author statement

Matic Pečovnik: Conceptualization, Methodology, Software, Validation, Formal analysis, Writing - Original Draft, Writing - Review & Editing, Visualization

Thomas Schwarz-Selinger: Conceptualization, Methodology, Formal analysis, Validation, Investigation, Resources, Writing - Review & Editing, Supervision, Funding acquisition

Sabina Markelj: Conceptualization, Writing - Review & Editing, Supervision, Funding acquisition